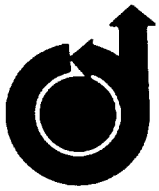

AIAA 79-1547R
Numerical Solution of Supersonic Laminar Flow over an Inclined Body of Revolution

C. M. Hung

Reprinted from
AIAA Journal
Volume 18, Number 8, August 1980, Page 921

AMERICAN INSTITUTE OF AERONAUTICS AND ASTRONAUTICS • 1290 AVENUE OF THE AMERICAS • NEW YORK, NEW YORK, N.Y. 10104

ARTICLE NO. 79-1547R

Numerical Solution of Supersonic Laminar Flow over an Inclined Body of Revolution

C. M. Hung*
NASA Ames Research Center, Moffett Field, Calif.

A mixed explicit-implicit scheme is used to solve the time-dependent thin-layer approximation of the Navier-Stokes equations for a supersonic laminar flow over an inclined body of revolution. Test cases for Mach 2.8 flow over a cylinder with 15-deg flare angle at angles of attack of 0, 1, and 4 deg are calculated. Good agreement is obtained between the present computed results and experimental measurements of surface pressure. A pair of vortices on the leeward and a peak in the normal force distribution near the flared juncture are predicted; the role of circumferential communication is discussed.

Nomenclature

A = right-hand side of Eq. (5)
C_{fx} = skin-friction coefficient along streamwise direction
c_v = specific heat at constant volume
D = diameter of cylindrical portion
E = total energy, $E = e_i + 0.5\ (u^2 + v^2 + w^2)$
F,G,H = transport inviscid flux vectors, Eq. (1)
G_v = transport viscous flux vector, Eq. (1)
L = length of cylindrical portion
L_ξ, L_η, L_ϕ = split finite difference operators in (ξ,η,ϕ)
$L_{\eta h}, L_{\eta p}$ = hyperbolic and parabolic operators in η direction
M_∞ = freestream Mach number
Pr = Prandtl number, 0.72
p = static pressure, $p = (\gamma - 1)\rho e_i$
p_∞ = freestream static pressure
Q = forcing terms in Eq. (1)
Q_ξ, Q_I, Q_v = split forcing terms in $L_\xi, L_{\eta h}, L_{\eta p}$
R = gas constant
Re_L = Reynolds number based on length L
r = radial direction
$r_b(x), r_f(x), r_o(x)$ = radius of body, fine mesh, and outer coarse mesh, respectively
t = time
$\Delta t, \Delta t_f$ = time increment of outer and inner meshes
U = conservative variables $(\rho, \rho u, \rho v, \rho w, \rho E)$
U' = variables in $L_{\eta p}$ operator $(u', v', w, u'^2, v'^2, w^2, e_i)$
u_∞ = freestream velocity
u,v,w = velocity components in (x,r,ϕ) coordinates
u', v' = transformed velocity components, $u' = v + v\tan\theta_i$; $v' = v - u\tan\theta_i$
x = axial direction
α = angle of attack
γ = ratio of specific heat, $\gamma = 1.4$
$(\Delta\eta)_{\min}$ = minimum fine mesh spacing
θ = flare angle
θ_i = $\tan^{-1}(r_b')$ local body slope angle
λ = second viscosity coefficient, $\lambda = -\frac{2}{3}\mu$
μ = molecular viscosity coefficient
ν = viscosity parameter in Eq. (5)
(ξ,η,ϕ) = transformed cylindrical coordinates
ρ = density
$\sigma_{xx}, \sigma_{rr}, \sigma_{rx}, \sigma_{\phi\phi}$ $\sigma_{r\phi}, \sigma_{\phi x}$ = thin-layer approximated viscous terms
Φ_x, Φ_r = energy dissipation and diffusion terms

Presented as Paper 79-1547 at the AIAA 12th Fluid and Plasma Dynamics Conference, Williamsburg, Va., July 23-25, 1979; submitted Aug. 6, 1979; revision received Jan. 3, 1980. This paper is declared a work of the U.S. Government and therefore is in the public domain.

Index categories: Boundary Layers and Convective Heat Transfer—Laminar; Supersonic and Hypersonic Flow; Computational Methods.

*Research Scientist. Member AIAA.

Introduction

SUPERSONIC flow over a body of revolution at angle of attack is of interest to both research and design engineers. A typical problem is to predict the nature of the three-dimensional flowfield around a cylinder with flared afterbody (Fig. 1). This configuration is seen in missiles, rockets, and space launch vehicles, in which the flare provides a natural fairing for multistage spacecraft or a simple means for shifting the center of pressure rearward and thereby improving the margin of static stability. It can also be used to simulate the underexpansion plume of rockets.

The pressure rises, due to the flare-shock, induce flow recirculation near the corner. At zero angle of attack, the flow is two-dimensional (axisymmetric) and the recirculation is closed as a toroid, provided the flow is steady. At angle of attack, the flare shock is stronger on the windward and weaker on the leeward. This variation of shock strength results in a pressure variation in the circumferential direction which induces a strong crossflow and makes the shock-wave and boundary-layer interaction highly three-dimensional. As the angle of attack increases, the crossflow first separates inside the recirculation region near the corner of the lee side. As the angle of attack is increased further, the crossflow also separates around the cylinder and the flare. Figure 2 shows a china clay laminar flow pattern and a sketched three-dimensional separation model experimentally observed by Ericsson et al.[1] and Fig. 3 shows a fluorescent oil visualization of a turbulent flow on a 23 deg cone frustum by Chyu and Coe.[2] Both figures indicate a circumferential communication and a pair or pairs of vortices shedding into the lee-side "wake."

Because of the complexity, previous theoretical and experimental studies considered the flare and lee-side

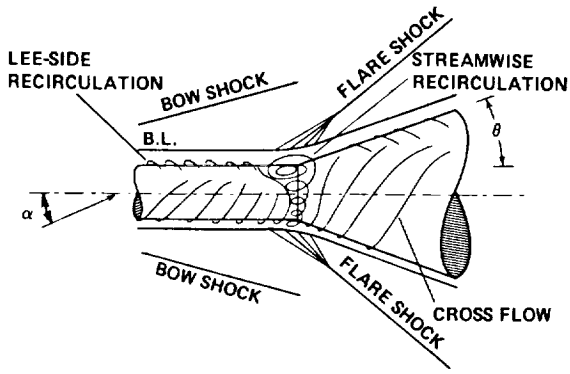

Fig. 1 Supersonic flows over cylinder with flare.

separations separately. The flare recirculation is studied as flow over a compression corner[3-5] and the lee-side separation is modeled as a flow over a cone.[6-8] To understand the detailed structure of the complete flowfield, however, the problem should be considered as a whole, and a complete three-dimensional problem must be solved.

In the present study, a rapid, mixed explicit/implicit numerical scheme[9] is used to solve the time-dependent thin-layer approximation of the three-dimensional Navier-Stokes equations for supersonic laminar flow over a hollow cylinder with a flare. The use of a hollow cylinder avoids the complication of prescribing the upstream boundary conditions. The objectives of this study are to investigate the three-dimensional shock-wave and boundary-layer interaction, to examine the associated three-dimensional separated flow structure, and to assess the role of circumferential communication in this interaction flowfield. The experiments conducted by Robinson[10] are selected for comparison at Mach number 2.8 and unit Reynolds number 0.3168×10^5/cm with various incident angles. Good agreement is obtained between the present computed results and experimental measurements of surface pressure and normal force distribution. The existence of a pair of vortices is also clearly observed.

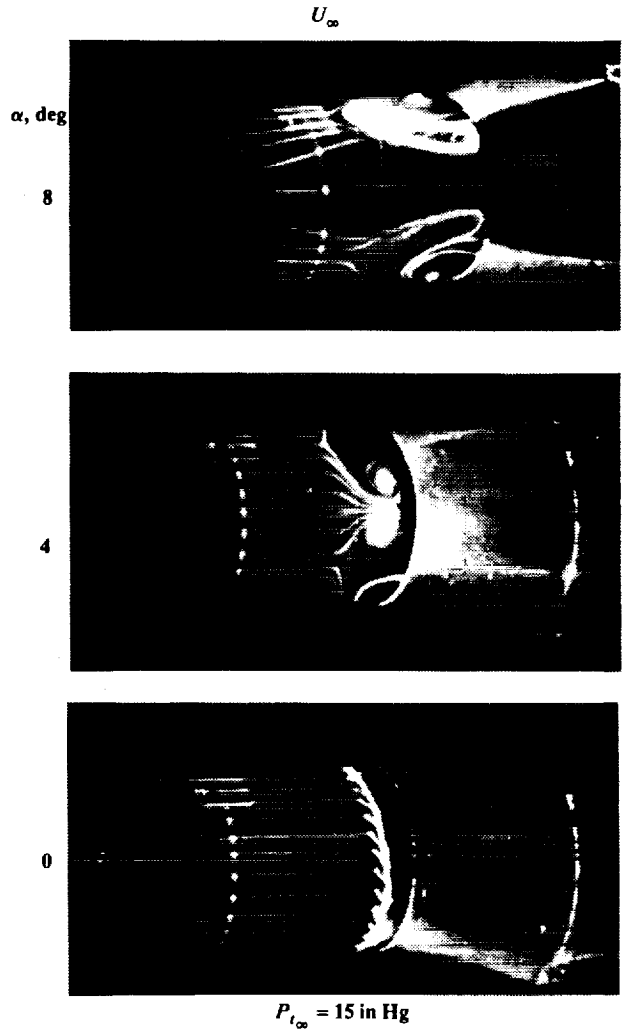

Fig. 3 Fluorescent oil studies on a cylinder with 23 deg cone frustrum.

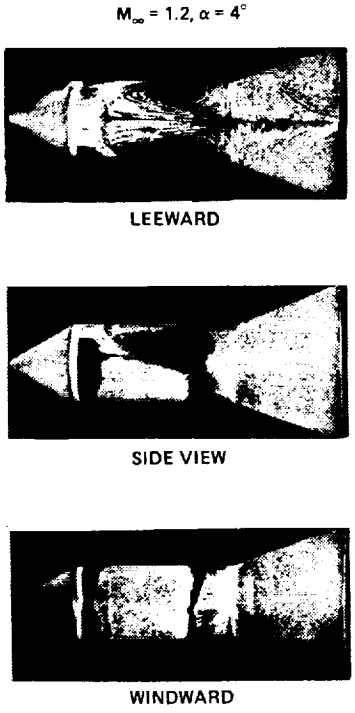

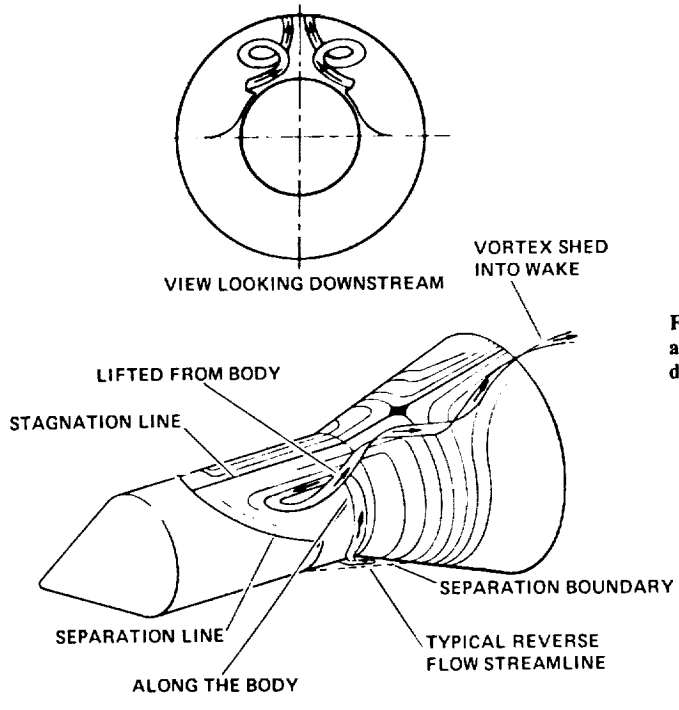

Fig. 2 A china clay flow pattern and a sketched three-dimensional model.

Analysis

Thin-Layer Approximation

Figures 4a and 4b show cross-sectional views of the computational domain in the (x,r) and (r,ϕ) planes. Here, θ is the cone half-angle of the flare. The flow is assumed to be symmetric in ϕ and hence only the half plane, 0 deg $\leq\phi\leq$ 180 deg, is needed. The mesh is uniformly spaced in both x and ϕ directions. In the r direction, a fine mesh spacing is used in the region near the body, $r_b\leq r\leq r_f$, to resolve the viscous forces, and a coarse mesh spacing is used in the outer region, $r_f<r<r_o$, where viscous effects are negligible.

The basic equations of the present analysis are the time-dependent compressible Navier-Stokes equations. In high Reynolds number flows, however, the viscous effects are confined near the wall boundary and are dominated by the viscous terms associated with the derivative in the direction normal to the wall. The viscous terms with the derivatives along the body are comparatively small and insignificant. This concept was first discussed by Prandtl in the development of boundary-layer theory and has been applied and extended to various techniques, such as the parabolized Navier-Stokes equations, or higher order boundary-layer theory for many complex flowfield calculations (cf., Refs. 7, 8, 11-13). The recent development of the thin-layer approximation[14] is based on that concept, with retention of all the unsteady and nonlinear inviscid terms of the Navier-Stokes equations. The retention of time-dependency in the governing equations, coupled with the direct inclusion of all inviscid terms in the calculation, permits the solution to progress naturally from an arbitrary initial condition to an asymptotic steady state and, hence, also permits an interaction flowfield to develop as time progresses. This approximation has been tested in the calculation of several flowfield problems and the results confirm its validity and applicability.[14-15] Consequently, the thin-layer approximation is used in the present study: All viscous terms associated with derivatives along the body are neglected while those with second-order derivatives across the thin layer alone are retained. Written in weak conservative form in transformed cylindrical coordinates, the thin-layer approximated Navier-Stokes equations are as follows:

$$\frac{\partial rU}{\partial t}+\frac{\partial rF}{\partial \xi}+\frac{\partial r(G-G_v)}{\partial \eta}+\frac{\partial rH}{r\partial\phi}+Q=0 \qquad (1)$$

where

$$\xi=x,\quad \eta=r-r_b(x),\quad v'=v-u\tan\theta_i$$

$$\tan\theta_i=r_b'(x)=0 \qquad \text{for } x\leq L$$

$$=\tan\theta \qquad \text{for } x>L$$

$$U=\begin{bmatrix}\rho\\ \rho u\\ \rho v\\ \rho w\\ \rho E\end{bmatrix}\quad F=\begin{bmatrix}\rho u\\ \rho u^2+p\\ \rho vu\\ \rho wu\\ (\rho E+p)u\end{bmatrix}\quad G=\begin{bmatrix}\rho v'\\ \rho uv'-p\tan\theta_i\\ \rho vv'+p\\ \rho wv'\\ (\rho E+p)v'\end{bmatrix}$$

$$H=\begin{bmatrix}\rho w\\ \rho uw\\ \rho vw\\ \rho w^2+p\\ (\rho E+p)w\end{bmatrix}\quad Q=\begin{bmatrix}0\\ 0\\ -p-\rho w^2+\sigma_{\phi\phi}\\ +\rho vw-\sigma_{r\phi}\\ 0\end{bmatrix}$$

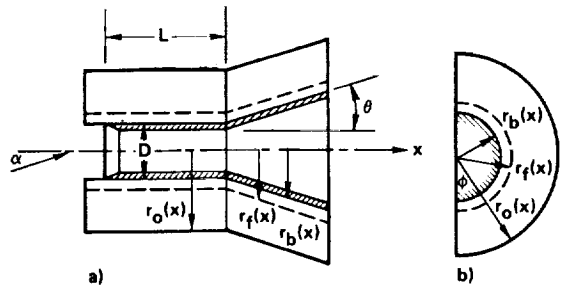

Fig. 4 Cross sections of the computational domain. a) (x,r) plane; b) (r,ϕ) plane.

$$G_v=\begin{bmatrix}0\\ \sigma_{rx}-\tan\theta_i\sigma_{xx}\\ \sigma_{rr}-\tan\theta_i\sigma_{rx}\\ \sigma_{r\phi}-\tan\theta_i\sigma_{\phi x}\\ \Phi_r-\tan\theta_i\Phi_x\end{bmatrix}$$

$$\Phi_x=\sigma_{xx}u+\sigma_{rx}v+\sigma_{\phi x}w-\frac{\gamma\mu}{Pr}\frac{\partial e_i}{\partial\eta}\tan\theta_i$$

$$\Phi_r=\sigma_{rx}u+\sigma_{rr}v+\sigma_{r\phi}w+\frac{\gamma\mu}{Pr}\frac{\partial e_i}{\partial\eta}$$

$$\sigma_{xx}=\lambda\frac{\partial}{\partial\eta}(v-u\tan\theta_i)-2\mu\frac{\partial u}{\partial\eta}\tan\theta_i$$

$$\sigma_{rr}=\lambda\frac{\partial}{\partial\eta}(v-u\tan\theta_i)-2\mu\frac{\partial v}{\partial\eta}$$

$$\sigma_{\phi\phi}=\lambda\frac{\partial}{\partial\eta}(v-u\tan\theta_i),\quad \sigma_{rx}=\mu\frac{\partial}{\partial\eta}(u-v\tan\theta_i)$$

$$\sigma_{r\phi}=\mu\frac{\partial}{\partial\eta}w,\quad \sigma_{\phi x}=-\mu\frac{\partial}{\partial\eta}w\tan\theta_i$$

Here (u,v,w) are velocity components in axial, radial, and azimuthal, (x,r,ϕ), directions; ρ,p, and E are density, pressure, and total energy, with $E=e_i+0.5\,(u^2+v^2+w^2)$, where e_i is the specific internal energy. The perfect gas relations are $p=(\gamma-1)\rho e_i$. The flow is assumed laminar and the molecular viscosity μ is evaluated by Sutherland's formula.

Time-Split Numerical Technique

The governing equations, Eqs. (1), are split into three groups corresponding to the coordinate directions for treatment by three operators, viz.,

$$L_\xi:\ \frac{\partial rU}{\partial\eta}+\frac{\partial rF}{\partial\xi}+Q_\xi=0$$

$$L_\phi:\ \frac{\partial rU}{\partial t}+\frac{1\partial rH}{r\partial\phi}=0$$

$$L_\eta:\ \frac{\partial rU}{\partial t}+\frac{\partial r(G-G_v)}{\partial\eta}+Q_I+Q_v=0$$

where

$$Q_\xi = \begin{bmatrix} 0 \\ -p\tan\theta_i \\ 0 \\ 0 \\ 0 \end{bmatrix} \quad Q_I = \begin{bmatrix} 0 \\ p\tan\theta_i \\ -p-\rho w^2 \\ \rho vw \\ 0 \end{bmatrix} \quad Q_v = \begin{bmatrix} 0 \\ 0 \\ \sigma_{\phi\phi} \\ -\sigma_{r\phi} \\ 0 \end{bmatrix}$$

The conventional two-step, explicit MacCormack scheme[16] is used in the L_ξ and L_ϕ operators and in the L_η operator for the outer coarse mesh region. In the fine-mesh inner region near the body, the L_η operator is split further into hyperbolic, $L_{\eta h}$, and parabolic, $L_{\eta p}$, operators for the inviscid and viscous terms,

$$L_{\eta h}: \quad \frac{\partial rU}{\partial t} + \frac{\partial rG}{\partial \eta} + Q_I = 0 \tag{2}$$

$$L_{\eta p}: \quad \frac{\partial rU}{\partial t} - \frac{\partial rG_v}{\partial \eta} + Q_v = 0 \tag{3}$$

Substitution of U and G in Eq. (2) yields

$$\left.\begin{aligned} \rho\left(\frac{\partial v'}{\partial t} + v'\frac{\partial v'}{\partial \eta}\right) + (1+\tan^2\theta_i)\frac{\partial p}{\partial \eta} &= \frac{\rho w^2}{r} \\ \left(\frac{\partial p}{\partial t} + v'\frac{\partial p}{\partial \eta}\right) + \gamma p\frac{\partial v'}{\partial \eta} &= -\frac{\gamma p v'}{r} \end{aligned}\right\} \tag{4}$$

Note that adding a term $p\tan\theta_i$ in Q_I and subtracting it in Q_ξ is for convenience in the derivation of Eq. (4).

In the $L_{\eta h}$ operator, Eq. (4) is solved for v' and p by the method of characteristics and then Eq. (2) is integrated in time from t to $t+\Delta t$ by the conventional predictor-corrector scheme with v' and p as known values at $t+\frac{1}{2}\Delta t$.

To compute the effect of the viscous terms in the inner region, Eq. (3) can be rewritten as

$$\frac{\partial \rho}{\partial t} = 0, \quad \frac{\partial U'}{\partial t} - \frac{1}{\rho r}\left(\nu r\sec^2\theta_i \frac{\partial U'}{\partial \eta}\right) = A \tag{5}$$

where

$$U' = \begin{bmatrix} u' \\ v' \\ w \\ u'^2 \\ v'^2 \\ w^2 \\ e_i \end{bmatrix} \quad A = \begin{bmatrix} -(\tan\theta_i/\rho r)\sigma_{\phi\phi} \\ -(1/\rho r)\sigma_{\phi\phi} \\ +(1/\rho r)\sigma_{r\phi} \\ -2A_1 \\ -2A_2 \\ -2A_3 \\ (A_1+A_2)\cos^2\theta_i + A_3 \end{bmatrix}$$

$$u' = u + \tan\theta_i v$$

$$A_1 = \frac{\mu}{\rho}\sec^2\theta_i\left(\frac{\partial u'}{\partial \eta}\right)^2 + \frac{\tan\theta_i}{\rho r}u'\sigma_{\phi\phi}$$

$$A_2 = (2\mu+\lambda)\frac{\sec^2\theta_i}{\rho}\left(\frac{\partial v'}{\partial \eta}\right)^2 + \frac{1}{\rho r}v'\sigma_{\phi\phi}$$

$$A_3 = \frac{\mu}{\rho}\sec^2\theta_i\left(\frac{\partial w}{\partial \eta}\right)^2 - \frac{1}{\rho r}w\sigma_{r\phi}$$

and ν is a viscosity parameter, equal to μ for elements u', w, u'^2, and w^2; equal to $(2\mu+\lambda)$ for elements v' and v'^2; and equal to $\gamma\mu/Pr$ for element e_i. The continuity equation has no viscous term and, hence, is trivial to solve. It implies that density is treated as a constant in time in the $L_{\eta p}$ operator. To avoid using a costly block-tridiagonal procedure, the total energy equation is split into three kinetic energy u'^2, v'^2, and w^2 equations and an internal energy equation. The kinetic energy equations are obtained by multiplying the corresponding momentum equations by u', v', and w, respectively, and the internal energy equation is obtained by subtracting the three kinetic energy equations from the total energy equation. Equation (5) is a parabolic model equation of diffusion, and can be efficiently solved by either a Crank-Nicolson or a first-order implicit difference with a simple tridiagonal inversion. The right-hand side of Eq. (5) is evaluated explicitly. In the present study, the u', v', and w are solved first and the new values of u', v', and w are then used to evaluate the dissipation terms A_1, A_2, and A_3 which in general may not be small. Details of the numerical method are discussed in Ref. 9.

The complete numerical procedure is expressed as:

$$U^{t+2\Delta t} = \underbrace{L_\xi(\Delta t)L_\phi(\Delta t)L_\eta(2\Delta t)L_\phi(\Delta t)L_\xi(\Delta t)}_{\text{Outer region}}$$

$$\times \underbrace{L_{\eta h}(\Delta t_f)L_{\eta p}(\Delta t_f)L_\xi(2\Delta t_f)L_\phi(2\Delta t_f)L_{\eta p}(\Delta t_f)L_{\eta h}(\Delta t_f)}_{\text{Inner region}}$$

$$\times \underbrace{L_{\eta h}(\Delta t_f)L_{\eta p}(\Delta t_f)L_\phi(2\Delta t_f)L_\xi(2\Delta t_f)L_{\eta p}(\Delta t_f)L_{\eta h}(\Delta t_f)}_{\text{Inner region}}$$

$$\times U^t$$

by which the solution is advanced two time steps from t to $t+2\Delta t$, where $2\Delta t_f = \Delta t$. The maximum stable time step, Δt, is determined by the CFL condition of the explicit operators.

Boundary Conditions

The coordinates are body-oriented and the flow at the upstream boundary is assumed to be uniform at supersonic freestream conditions $(M_\infty, u_\infty, p_\infty, \rho_\infty)$. The angle of attack is imposed by setting the upstream velocity components as $u = u_\infty\cos\alpha, v = u_\infty\sin\alpha\cos\phi$, and $w = u_\infty\sin\alpha\sin\phi$. The downstream and far-field boundaries are positioned far enough from the three-dimensional interaction region that zero-gradient boundary conditions can be used. The symmetry condition is applied at $\phi = 0$ and 180 deg planes. The wall is assumed impermeable and no-slip boundary conditions are used. The wall is taken to be either isothermal or adiabatic, and the wall pressure is evaluated using

$$\frac{\partial p}{\partial \eta} = 0 \text{ at } \eta = 0$$

For our present case, the first mesh point is so close to the wall that this pressure condition is appropriate. During the calculations within the inner mesh, the flux and stress terms at the internal boundary, $r = r_f(x)$, are saved, and their net quantities are then used as boundary conditions for the outer mesh flow calculations.

Results and Discussion

The experiments selected for comparison were conducted by Robinson.[10] The flow conditions are $M_\infty = 2.8$; $Re_L = 0.8\times10^6$; $\theta = 15$ deg; $D = 101.6$ mm; $L = 252.5$ mm; and $\alpha = 0$, 1, and 4 deg. The wall is assumed adiabatic. A grid of

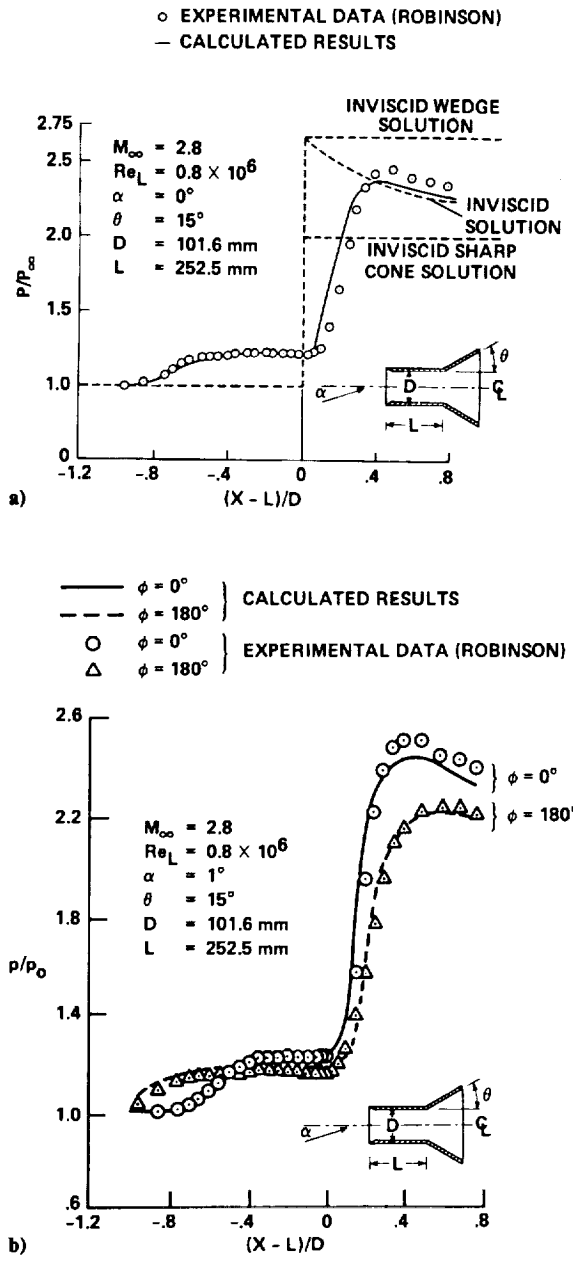

Fig. 5 Comparison of surface pressure. a) $\alpha = 0$ deg; b) $\alpha = 1$ deg; c) $\alpha = 4$ deg.

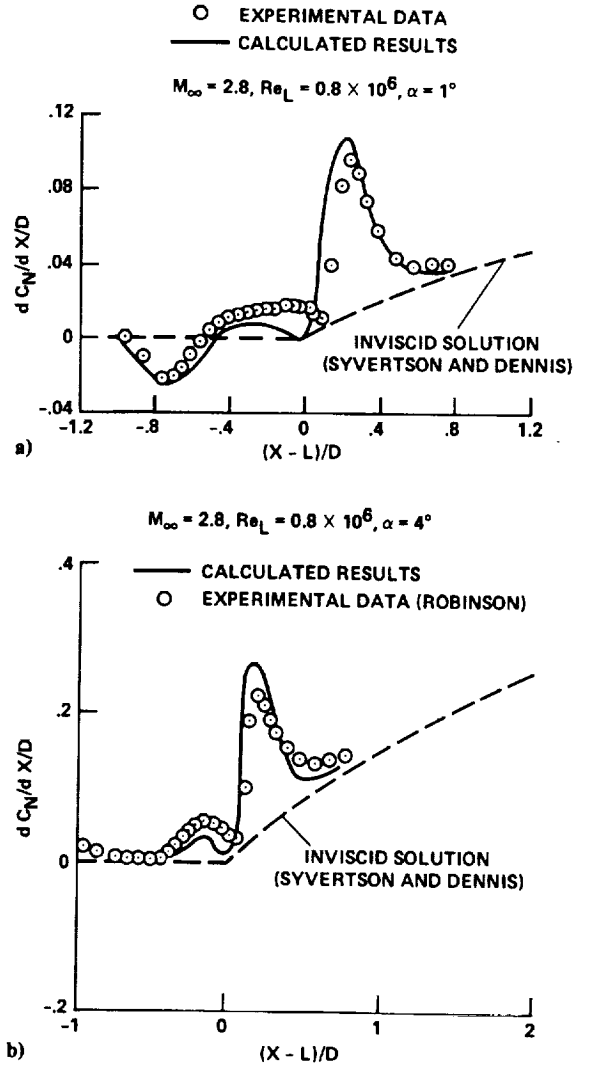

Fig. 6 Comparison of normal force distribution. a) $\alpha = 1$ deg; b) $\alpha = 4$ deg.

$$\left(\frac{dC_N}{dx/D} = \frac{4}{\pi}\frac{2r_b}{D}\int_0^{\pi}\frac{2p}{\rho_\infty u_\infty^2}\cos\phi\, d\phi\right)$$

$(45 \times 34 \times 20)$ encloses a computational domain of

ξ/L: from -0.0156 to 1.3702

η/D: from 0 to 1.2338

ϕ: from 0 to 180 deg

A geometrically stretched fine mesh, 20 points in η-direction, is used near the body to $\eta/D = 0.1397$, with a minimum mesh spacing $(\Delta\eta)_{\min} = 0.5\, L/\sqrt{Re_L}$.

Figures 5a-5c show comparisons of the present computed results with experimental measurements of surface pressure for three incident angles: $\alpha = 0$, 1, and 4 deg. The agreement is very good. Also shown in Fig. 5a are the inviscid solutions for a sharp cone, two-dimensional wedge, and cylinder-flare, respectively. In Fig. 5b, two meridian angles, $\phi = 0$ and 180 deg, and in Fig. 5c, three meridian angles $\phi = 0$, 90, and 180 deg, are shown. The inviscid solutions shown in Fig. 5c were calculated by adding a 30 deg cone in front of the cylinder and are presented to indicate the viscous effects at two meridian angles, $\phi = 0$ and 180 deg.

Note that, at an angle of attack, the "effective" flare angle is larger on the windward and smaller on the leeward. If there

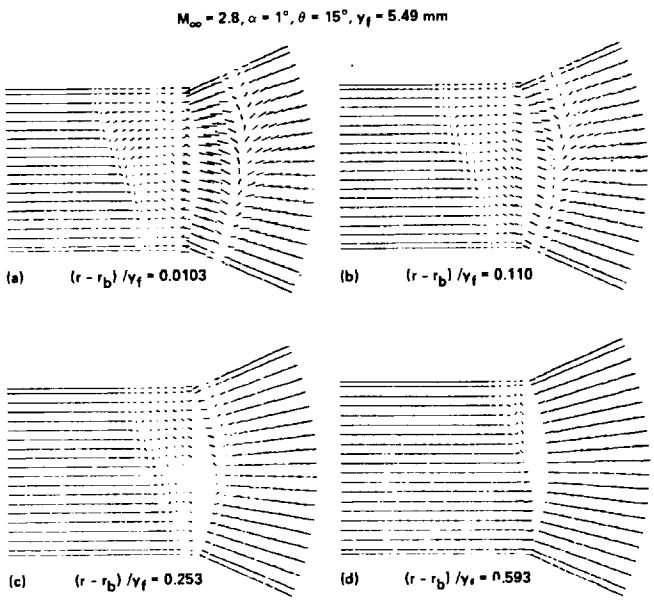

Fig. 7 Unwrapped velocity plots (u' and w) for $\alpha = 1$ deg.

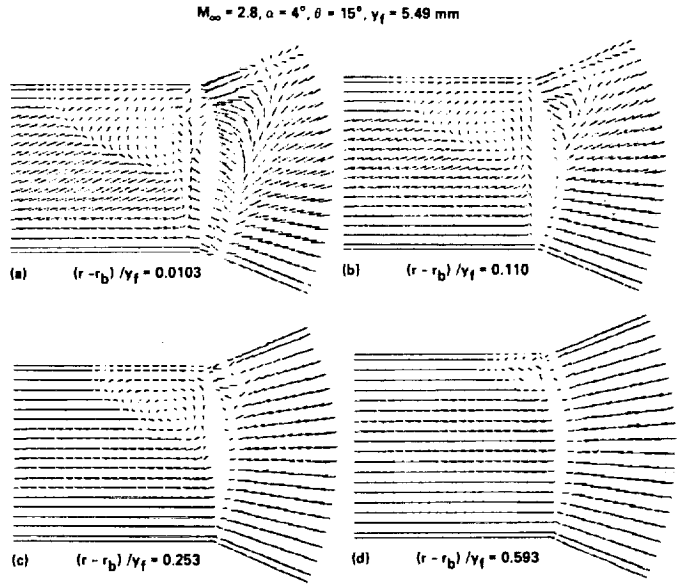

Fig. 8 Unwrapped velocity plots (u' and w) for $\alpha = 4$ deg.

were no circumferential communication or crossflow, the streamwise recirculation should be larger on the windward and smaller on the leeward. The existence of circumferential communication by means of convention and diffusion of crossflow, however, makes the flowfield behave oppositely. The crossflow sweeps much of the low-momentum fluid from the windward boundary layer to the leeward. This process results in thinning and strengthening the windward boundary layer, while at the same time thickening and weakening the leeward boundary layer. Near the cylinder-flare juncture the communication is more efficient and effective. While the flare shock retards the flow, inducing streamwise recirculation, the crossflow is stronger and the swept fluid indeed can be carrying "negative" momentum. Overall, it leads to a forward movement of separation on the leeward and an aft movement on the windward, as can be seen in the pressure rises and plateaus shown in Figs. 5b and 5c. Similar effects were also observed by Deep[17] in an experimental study of shock-induced separation on a cone-cylinder frustum.

It is interesting to note that, due to the thickening of the boundary layer and the larger separation on the leeward, the

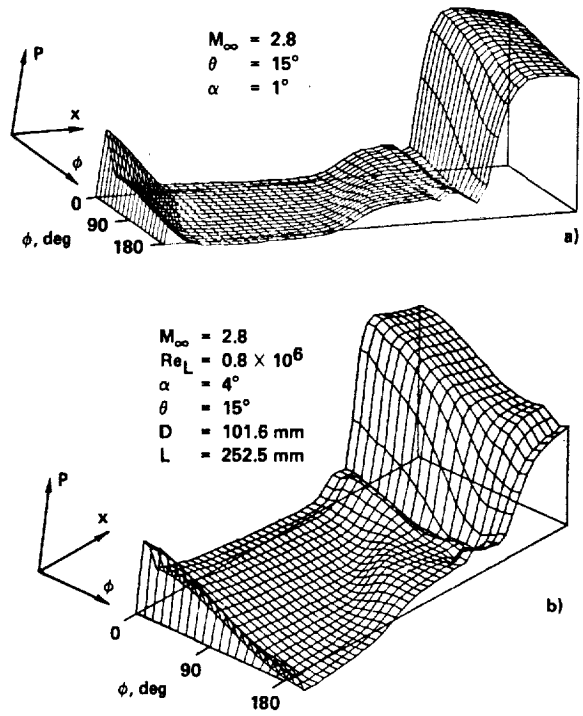

Fig. 9 Three-dimensional plots of surface pressure.

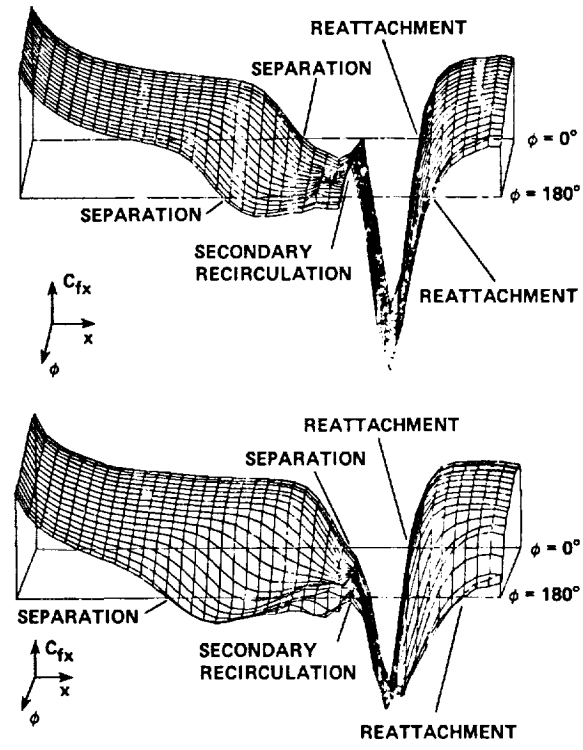

Fig. 10 Three-dimensional plots of skin friction along streamwise direction.

leeward surface pressure rises gradually and shows a substantial difference from the inviscid solution, while the windward surface pressure rises sharply and shows less viscous effects. This results in a peak of normal force distribution near the flare juncture, as shown in Figs. 6a and 6b. Also shown in the figures are inviscid solutions using the Syvertson and Dennis[18] shock expansion method. At small angle of attack, $\alpha = 1$ deg, the surface pressure on the leeward can be higher than that on the windward (Fig. 5b) near the streamwise separation point on the lee side, which causes a

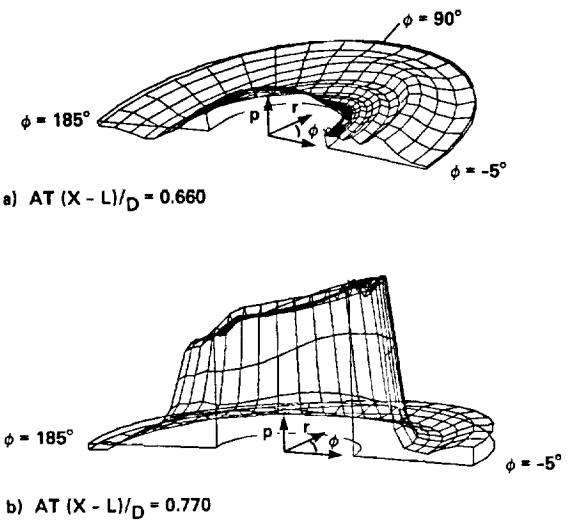

Fig. 11 Plots of static pressure on $(r-\phi)$ planes at two $x-$ locations.

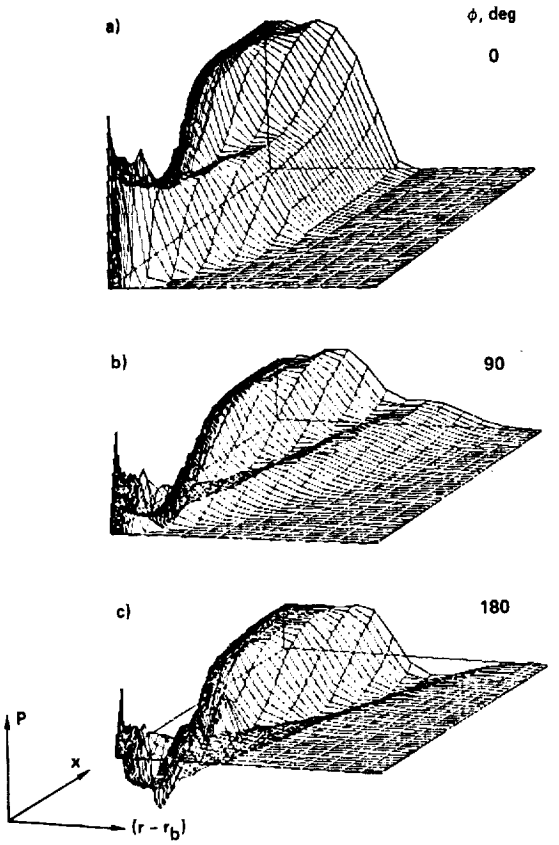

Fig. 12 Plots of static pressure on $(x-r)$ planes at three meridian angles.

small negative normal force distribution in front of the flare (Fig. 6a). In general, the present computed results closely predict the basic features observed by the experiments.

Figures 7 and 8 show unwrapped velocity plots, u' vs w, at several radial levels for two incident angles, respectively. They clearly indicate the variation of streamwise recirculation with meridian angle.

One of the most striking features is that, due to the combination of streamwise recirculation and lee-side crossflow separation, there exists a pair of vortices which become stretched and are shed into the "wake." At small incidence, $\alpha = 1$ deg, the vortex is weak and not clear. At $\alpha = 4$ deg, a pair of vortices is clearly formed and the feature is very similar to the experimental observation of Ericsson et al.[1] shown in Fig. 2. A similar vortex pattern has also been observed on the nose of an inclined hemisphere-cylinder by Hsieh and Wang.[19]

The variations of surface pressure and streamwise skin-friction coefficient are shown in Figs. 9 and 10. Note that both Figs. 10a and 10b indicate a small secondary recirculation in the η direction around the lee side. This type of secondary recirculation has been observed in many three-dimensional experiments; see, for instance, Ref. 20. But in the present study, since there is a small pressure oscillation (see Figs. 9a and 9b) associated with numerical error due to body discontinuity and sharp pressure rise near the juncture, the observation is inconclusive and further investigation with better mesh resolution is needed. Figure 11 shows plots of static pressure fields on $(r-\phi)$ planes at two x locations and Fig. 12 shows those on $(x-r)$ planes at three meridian angles: $\phi = 0$, 90, and 180 deg. At $\phi = 90$ and 180 deg (Figs. 12b and 12c) a strong overexpansion, coupled with the leading edge and flare-shock compression, is clearly shown.

The three-dimensional program is coded in such a way as to permit treatment of a general body of revolution, with $r_b = f(x)$. In the present numerical procedure for computation based on the thin-layer approximation, the program requires 0.00048 s per grid point per time-step on a CDC 7600. With a grid of $45 \times 34 \times 20$, it takes about 1.25 h of computation time for a converged steady solution. The option of solving the complete Navier-Stokes equations is also coded; it requires about 25% more computation time. For the present cases, results from the thin-layer approximation and the complete Navier-Stokes equations agree within 3%.

Concluding Remarks

A supersonic laminar flow over an inclined body of revolution has been numerically calculated. The time-dependent compressible Navier-Stokes equations, with and without a thin-layer approximation, were solved by a rapid, mixed explicit-implicit numerical scheme. Good agreement was obtained between computed and experimental results for surface pressure at different meridian angles and normal force distribution. The results show that the crossflow: 1) effectively transfers low or negative momentum fluid to the leeward; 2) causes small separation on the windward and large separation on the leeward; 3) leads to a sharp pressure rise on the windward, and a smooth turning of streamlines and a gradual pressure rise on the leeward; and 4) results in a peak in the normal force distribution near the cylinder-flare juncture, and a pair of vortices on the leeward.

References

[1] Ericsson, L. E., Reding, P., and Guenther, R. A., "Analytic Difficulties in Predicting Dynamic Effects of Separated Flow," *Journal of Spacecraft and Rockets*, Vol. 8, Aug. 1971, pp. 872-878.

[2] Chyu, W. J. and Coe, C. F., private communication, Moffett Field, Calif..

[3] Kuehn, D. M., "Laminar Boundary-Layer Separation Induced by Flare on Cylinder at Zero Angle-of-Attack," NASA TR R-146, 1962.

[4] Nielsen, J. H., Lynes, L. L., and Goodwin, F. K., "Theory of Laminar Separated Flows on Flared Surfaces Including Supersonic Flow with Heating and Cooling," *AGARD Conference Proceedings No. 4, Separated Flow*, 1966.

[5] Lees, L. and Reeves, B. L., "Supersonic Separated and Reattaching Laminar Flow. I. General Theory and Application to Adiabatic Boundary-Layer/Shock-Wave Interaction," *AIAA Journal*, Vol. 2, Nov. 1964, pp. 1907-1920.

[6] Stetson, K. F., "Boundary-Layer Separation on Slender Cones at Angle-of-Attack," *AIAA Journal*, Vol. 10, May 1972, pp. 642-648.

[7] Lubard, S. C. and Helliwell, W. S., "Calculation of the Flow on a Cone at High Angle-of-Attack," *AIAA Journal*, Vol. 12, Feb. 1971, pp. 277-284.

[8] Lin, T C. and Rubin, S. G, "Viscous Flow Over a Cone at Moderate Incidence, Part. 2: Boundary Layer," *Journal of Fluid Mechanics*, Vol. 59, July 1973, pp. 593-620.

[9] MacCormack, R. W., "An Efficient Numerical Method for Solving the Time-Dependent Compressible Navier-Stokes Equations at High Reynolds Number," NASA TM X-73-129, July 1976.

[10] Robinson, M. L., "Boundary Layer Effects in Supersonic Flow over Cylinder-Flare Bodies," Australian Defense Scientific Service, Weapons Research Establishment, Salisbury, South Australia, WRE-Rept.-1238 (WR&D), July 1974.

[11] Cheng, H. K., Chen, S. Y., Mobley, R., and Huber, C. R., "The Viscous Hypersonic Slender-Body Problem: A Numerical Approach Based on a System of Composite Equations," The Rand Corp., Santa Monica, Calif., RM 6193-PR, May 1970.

[12] McDonald, H. and Briley, W. R., "Three-Dimensional Supersonic Flow of a Viscous or Inviscid Gas," *Journal of Computational Physics*, Vol. 19, Oct. 1975, pp. 150-178.

[13] Davis, R. T., "Numerical Solution of the Hypersonic Viscous Shock-Layer Equations," *AIAA Journal*, Vol. 8, May 1970, pp. 843-851.

[14] Pulliam, T. H. and Steger, J. L., "Implicit Finite-Difference Simulation of Three-Dimensional Compressible Flow," AIAA Paper 78-10, Huntsville, Ala., Jan. 1978.

[15] Baldwin, B. S. and Lomax, H., "Thin Layer Approximation and Algebraic Model for Separated Turbulent Flows," AIAA Paper 78-257, Huntsville, Ala., Jan. 1978.

[16] MacCormack, R. W. and Baldwin, B. S., "A Numerical Method for Solving the Navier-Stokes Equations with Application to Shock-Boundary Layer Interactions," AIAA Paper 75-1, Pasadena, Calif., Jan. 1975.

[17] Deep, R. A., "Experimental Study of Shock-Induced Separation on Cone-Cylinder-Conical Frustum Body of Revolution," Redstone Arsenal Rept. 6M86, Huntsville, Ala., Dec. 1955.

[18] Syvertson, C. A. and Dennis, D. H., "A Second-Order Shock-Expansion Method for Applicable to Bodies of Revolution Near Zero Lift," NACA Rept. 1328, 1957.

[19] Hsieh, T. and Wang, K. C., "Concentrated Vortex on the Nose of N Inclined Body of Revolution," *AIAA Journal*, Vol. 14, May 1976, pp. 698-700.

[20] Bachalo, W. D., "Experiments on Supersonic Boundary-Layer Separation in Three Dimensions," *Journal of Applied Mechanics, Transactions of ASME*, Series E, Vol. 42, June 1975, pp. 289-294.